

In-cavity soliton self-frequency shift ultrafast fiber lasers

JUNSONG PENG,^{1,2} HAO LUO,¹ AND LI ZHAN^{1,*}

¹State Key Laboratory of Advanced Optical Communication Systems and Networks, Shanghai Jiao Tong University, Shanghai 200240, China

²State Key Laboratory of Precision Spectroscopy, East China Normal University, Shanghai 200062, China

*Corresponding author: lizhan@sjtu.edu.cn

Received 24 October 2018; revised 10 November 2018; accepted 19 November 2018; posted 20 November 2018 (Doc. ID 349146); published 3 December 2018

Lasing wavelengths are generally limited at the gain bands of active materials. In this Letter, we propose and demonstrate a new concept of ultrafast fiber laser based on in-cavity soliton self-frequency shift (SSFS). Benefiting from SSFS, the wavelength of ultrafast fiber lasers can be beyond the gain band of active fibers. SSFS was previously stimulated by transmitting pulses in passive fibers. Triggering SSFS inside a laser cavity has never been reported. We successfully stimulate SSFS in a laser by employing a piece of dispersion-shifted fiber. In-cavity SSFS is expected to be implemented in various ultrafast lasers and is conducive to develop compact wavelength versatile laser sources. © 2018 Optical Society of America

<https://doi.org/10.1364/OL.43.005913>

Ultrafast fiber lasers have been studied and developed extensively [1–7]. However, a fundamental limitation is that the lasing wavelength always locates in the gain band of active media. Producing new wavelength pulses is not only scientifically interesting, but also attractive for various applications, which constitutes a basic research topic in the laser community. Exploring new doping material is a possible solution. On the other hand, optical nonlinear effects promise an alternative proposal to generate new wavelength pulses. Soliton self-frequency shift (SSFS) is a well-known nonlinear phenomenon in optics; that is, the wavelength of a soliton propagating in a Raman-active medium like optical fiber is redshifted because the low frequency of the soliton spectrum experiences Raman gain at the expense of the high-frequency. SSFS has drawn much attention due to its wide-range applications [8] such as wavelength tuning [9], soliton trapping [10], resonant radiation [11], and nonlinear images [12–14]. To date, all previous studies referring to SSFS generation were achieved by transmitting a soliton along a piece of passive fiber. Whether or not SSFS can be directly generated in a laser oscillator is of fundamental interest in the laser community.

In this Letter, we manipulate SSFS generation in a mode-locked fiber laser oscillator to output ultrafast pulses. The lasing wavelength can be shifted beyond the gain band

of an erbium-doped fiber (EDF). SSFS is generated by employing a piece of dispersion-shifted fiber (DSF) in the cavity. It is observed when the pump power is above a threshold, evidenced by a 50 nm wavelength shift from the mode-locked pulses without SSFS. The conversion efficiency from the standard mode-locked pulses to the SSFS pulses increases with the length of the DSF. SSFS does not occur if the length of the DSF is below a threshold. Numerical simulations confirm the experimental observations.

Figure 1 shows the configuration of our SSFS fiber laser. The ring cavity is made of a 2.2 m EDF (OFS-80), pumped by two 980 nm laser diodes through wavelength division multiplexers (WDMs). A polarization dependent isolator (PDI) sandwiched between two polarization controllers (PC1 and PC2) is used as the mode-locking component. A piece of the DSF is added to enhance the Raman effect for SSFS, and two optical couplers (OC1 and OC2) are used to observe the dynamics of SSFS. One (1:99) with an output ratio of 1% is placed before the DSF to monitor the seed pulse; the other (10:90) is located after the DSF. To avoid multi-pulsing effectively, the cavity is dispersion managed. The EDF has normal dispersion, and the DSF has anomalous dispersion, which are 63.8 and $-10 \text{ ps}^2/\text{km}$ at 1557 nm, respectively. Large

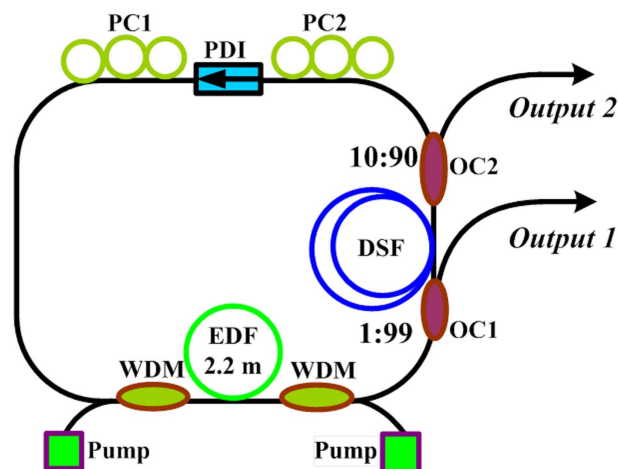


Fig. 1. Experimental configuration of the laser.

intracavity power is extracted through the 90% port of OC2, which also contributes to suppressing the multi-pulsing. The DSF has less second-order dispersion than a standard single-mode fiber (SMF), resulting in less temporal broadening. In addition, the smaller mode-field diameter of the DSF (8.35 μm) also helps to increase the nonlinearity for SSFS. The length of the DSF was varied from 4 to 104 m during the experiment for a systematic investigation. The spectrum is measured by AQ6370-B. The autocorrelation trace is measured by FR-103XL.

Mode locking was initiated by nonlinear polarization rotation (NPR), which relies on intensity dependent rotation of an elliptical polarization state in the fiber [15]. With proper settings of the initial polarization ellipse and phase bias, pulse shortening occurs. The mode-locking threshold is 171 mW of the pump power. Figure 2 shows the spectra scaling with the pump power at output 2 with a DSF length of 60 m. The total cavity length is 68 m corresponding to a pulse repetition rate of 2.94 MHz, as observed on an oscilloscope. As depicted in Fig. 2, when the pump power is below 706 mW, there is no SSFS. The spectral component around 1530 nm is caused by amplified spontaneous emission (ASE), which is common in a long-cavity fiber laser arising from the gain recovery of the EDF [16]. Remarkably, when the pump power is increased to 760 mW, the spectrum changes significantly. A new wavelength component centered at 1600 nm appears. It is important to note that this redshifted component is generated by SSFS. First, it is generated when the pump power exceeds a threshold. This is consistent with the fact that there is a threshold for SSFS generation [17]. Secondly, the redshifted spectrum by SSFS corresponds to a soliton whose spectrum is Sech^2 -like. This is examined by Sech^2 function fitting in Fig. 3. The good fitting indicates that the pulses are solitons. Thirdly, the wavelength separation between the seed pulse and the new soliton depends on the pump power [17,18]. In Fig. 2, the central wavelength of the seed pulse is invariant with the increasing of the pump power (171–706 mW), but one of the new solitons shifts to the right by 2 nm, as the pump power is increased from 760 mW to 1.32 W. This indicates that the separation between the two is pump power dependent, consistent with the theory of SSFS. Besides, the spectral width of the new soliton increases

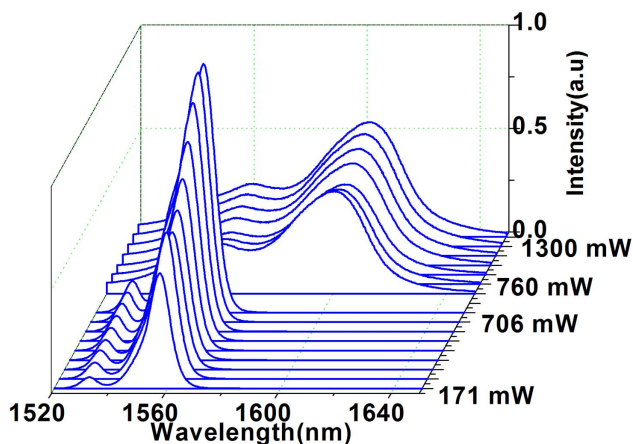


Fig. 2. Spectra scaling with pump power at output 2 when the length of the DSF is 60 m.

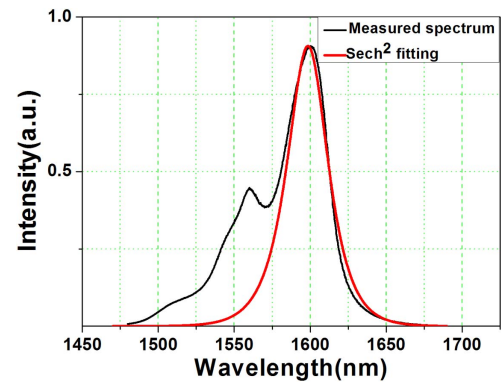


Fig. 3. Spectrum (black) and Sech^2 fitting (red) at output 2.

from 35.5 to 36.8 nm, as the pump power is tuned from 760 mW to 1.32 W, which is also consistent with SSFS dynamics [19]. If higher pump power is applied, the spectral width could be further increased. SSFS is common when the seed pulse is subpicosecond. If the pulse is too short, other nonlinear effects such as self-phase modulation (SPM) dominate the pulse evolution. In our laser, the spectral width of seed pulses is ~ 13 nm corresponding to a chirp-free pulse of ~ 250 fs. As the laser is dispersion managed, the pulse is chirped in the cavity [20]. It is estimated to be 900 fs before entering the DSF, which is in the range for SSFS generation [17].

To examine the dynamics of SSFS in the cavity, the pulse spectrum before the DSF is measured (output 1 in Fig. 1) when SSFS is generated, as shown in Fig. 4. The spectrum around 1600 nm (Fig. 4) is much weaker than that in Fig. 2, meaning that SSFS becomes pronounced after the pulse propagates down the DSF, as expected. Although the redshifted component is strong in the end of the DSF, it is attenuated extensively when propagating further in the EDF (implied by Figs. 2 and 4), as it is beyond the gain band of the EDF.

The physic processes in the laser are clear. First, ultrashort pulses are generated through mode locking. The pulse then propagates in the DSF, in which the Raman effect is enhanced. SSFS results in shifting the wavelengths of pulses. The seed pulses in Fig. 2 are not totally transferred to the new solitons. The conversion efficiency denoted by ratio of the SSFS pulse to the total energy of the light field should be proportional to the

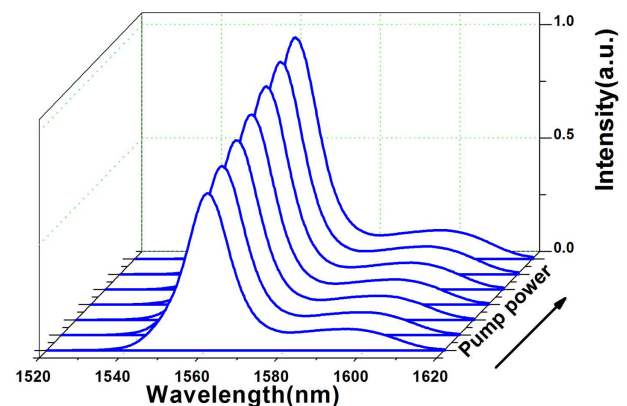


Fig. 4. Spectra at output 1 with the pump power increasing from 760 mW to 1.3 W when SSFS is stimulated.

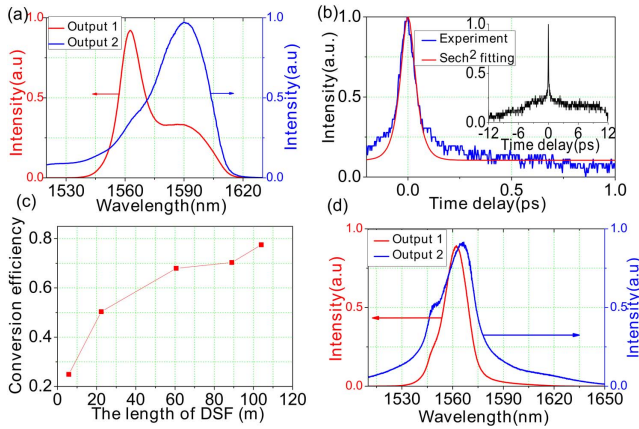


Fig. 5. (a) Spectra from output 1 (red) and output 2 (blue) under the maximum pump power when the DSF is 104 m. (b) Corresponding autocorrelation trace of the pulse measured at output 2 (blue) and Sech^2 fitting (red); the inset is the autocorrelation trace measured in a long time range. (c) Conversion efficiency of SSFS versus the length of the DSF. (d) Spectra from output 1 (red) and output 2 (blue) when the length of the DSF is 4 m, showing no evidence of SSFS.

length of the DSF. We examine this relationship by increasing the length of the DSF to 104 m. The pulse spectrum measured at the maximum pump power is shown in Fig. 5(a). The red curve is the one observed at output 1, and the blue one is the spectrum measured at output 2. It can be seen that the spectrum of the seed pulse is converted to the redshifted component almost completely. The autocorrelation trace of the pulses in Fig. 5(a) is shown in Fig. 5(b), which is obtained by optimizing the length of the SMF outside the cavity. The autocorrelation trace is close to a Sech^2 fitting. The inset shows the same trace in a long time range. The pulse is 85 fs assuming a Sech^2 profile. The pulse width before compression is 136 fs. Considering the spectral width of 33 nm, the time-bandwidth product is 0.332, which is close to that of a soliton. The background in the autocorrelation trace is caused by ASE noise and third-order dispersion [the inset of Fig. 5(b)].

In contrast, the conversion efficiency decreases as the DSF length is decreased, and SSFS does not occur once the length of the DSF is below a threshold. Figure 5(c) shows the conversion efficiency variation with the length of the DSF. Figure 5(d) demonstrates that SSFS disappears when the DSF is reduced to 4 m. The spectral width of the seed pulses (red) is 29 nm in Fig. 5(d), but it is 13 nm when SSFS is generated. In other words, the pulse duration in Fig. 5(d) is much shorter than that for generating SSFS; hence, only SPM appears [blue curve in Fig. 5(d)]. To further prove the importance of the DSF, it is replaced by a piece of the 100 m SMF. Such a length is nearly the same as the length of the DSF used in Fig. 5(a). In this case, SSFS is not observed, as the spectrums from the two output ports are not redshifted. The low dispersion and high nonlinear coefficient of the DSF are important for SSFS generation.

To verify the laser operation, a numerical study was carried out. The governing equation was evaluated by using split-step Fourier methods. In the simulation, dispersion, nonlinearity, gain saturation, Raman scattering, and the saturable

absorber effect were taken into consideration. The governing equation is [21]

$$\frac{\partial A}{\partial z} = -\frac{1}{2}(i\beta_2)\frac{\partial^2 A}{\partial \tau^2} + \frac{1}{6}\beta_3\frac{\partial^3 A}{\partial \tau^3} + i\gamma|A|^2A + gA + i\gamma T_R\frac{\partial|A|^2}{\partial \tau}A, \quad (1)$$

where A is the envelope of the field, z is the propagation coordinate, τ is time scaled to the pulse duration, Υ is the non-linear fiber coefficient, β_2 and β_3 are the second- and third-order dispersion, respectively. $g = g_0 \exp(-E_p/E_s)$ is the gain of the EDF, where g_0 , E_p , and E_s are the small-signal gain, the pulse energy, and the gain saturation energy, respectively. $T_R = 5$ fs is related to the Raman gain. The NPR mode-locking mechanism is described by an intensity-dependent transmission function:

$$T(\tau) = R_0 + \Delta R \left(1 - \frac{1}{1 + P/P_0} \right), \quad (2)$$

where R_0 is unsaturable loss, ΔR is saturable loss, P is the instantaneous pulse power, and P_0 is saturable power. In the simulation, the following parameters are chosen: $g_0 = 4.05/\text{m}$, $E_s = 1 \times 10^{-11}$ J, $\Delta R = 95\%$, $R_0 = 5\%$, and $P_0 = 40$ mW. β_2 and β_3 of the EDF and DSF are $63.8 \text{ ps}^2/\text{km}$, $0 \text{ ps}^3/\text{km}$, $-10 \text{ ps}^2/\text{km}$, and $0.1 \text{ ps}^3/\text{km}$, respectively. The length of the DSF used is 104 m, which is the same as the experimental value used in obtaining Fig. 5(a).

Figure 6 shows the pulse spectrum obtained in the simulation. The blue curve is the pulse spectrum without Raman gain, and the red curve is the one with Raman gain. The central wavelength of the blue curve is 1565 nm, which is in the gain band of the EDF. In contrast, the wavelength of the red curve shifts to the longer side as a result of Raman gain. The temporal widths are the same in the two cases, as the dispersion is fixed. In experiments, the dispersion varies along the laser cavity: the WDM, EDF, OC1, DSF, OC2, and PDI have different dispersion values. This dispersion variation reduces the phase-matching condition of interference between the continuum wave and the soliton, suppressing Kelly sidebands generation. However, for simplicity, only the EDF and DSF are included in the numerical study, and the net dispersion is anomalous, giving rise to Kelly sideband generation in

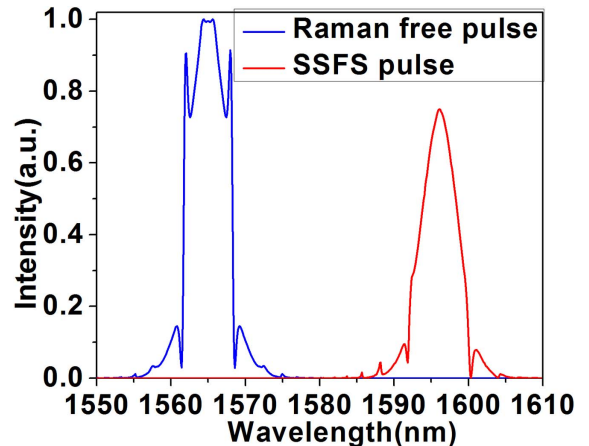


Fig. 6. Pulse spectrum with (red) and without (blue) Raman gain from the numerical simulation.

Fig. 6 (blue). The simulated SSFS pulse energy is ~ 40 pJ, which is close to that of a fundamental soliton. In the experiment, there is a pump power threshold for stimulating SSFS. The numerical study also shows that SSFS only occurs when the gain saturation energy of the EDF reaches a threshold value, and solitons without wavelength shifts are generated if the gain saturation energy is below this threshold. The numerical results are in agreement with the experiments, demonstrating the formation mechanism of SSFS pulses. It is worthwhile to note that the simulation results depend on the initial input field in long-cavity mode-locked fiber lasers [22]. The one used in our simulation is quantum noise.

In conclusion, we propose and demonstrate an in-cavity SSFS fiber laser for the first time, to the best of our knowledge. The central wavelength of the laser can break through the limit of the gain band of active fibers. This proposal can be widely used in fiber lasers with different gain media. Here we operate the SSFS laser at the EDF band. However, it can also be applied in Yb-doped, Tm-doped fiber lasers, and so on. Besides, the method can be realized in solid-state lasers, as long as the Raman medium is employed. Besides soliton lasers, there are other types of ultrafast fiber lasers such as similariton lasers [23] and normal dispersion fiber laser [24]. Exploring SSFS in these lasers is of great importance to extend their wavelength range.

Funding. National Natural Science Foundation of China (NSFC) (11704123, 11874040, 61775059); Foundation for leading talents of Minhang, Shanghai.

REFERENCES

1. B. Oktem, C. Ulgudur, and F. O. Ilday, *Nat. Photonics* **4**, 307 (2010).
2. M. E. Fermann and I. Hartl, *Nat. Photonics* **7**, 868 (2013).
3. H. Luo, L. Zhan, L. Zhang, Z. Q. Wang, C. X. Gao, and X. Fang, *J. Lightwave Technol.* **35**, 3780 (2017).
4. W. Fu, L. G. Wright, and F. W. Wise, *Optica* **4**, 831 (2017).
5. W. Fu, L. G. Wright, P. Sidorenko, S. Backus, and F. W. Wise, *Opt. Express* **26**, 9432 (2018).
6. P. Ryczkowski, M. Närhi, C. Billet, J. M. Merolla, G. Genty, and J. M. Dudley, *Nat. Photonics* **12**, 221 (2018).
7. Z. Q. Wang, L. Zhan, A. Majeed, and Z. X. Zou, *Opt. Lett.* **40**, 1065 (2015).
8. J. H. Lee, J. van Howe, C. Xu, and X. Liu, *IEEE J. Sel. Top. Quantum Electron.* **14**, 713 (2008).
9. N. Nishizawa and T. Goto, *IEEE J. Sel. Top. Quantum Electron.* **7**, 518 (2001).
10. N. Nishizawa and T. Goto, *Opt. Lett.* **27**, 152 (2002).
11. H. Luo, L. Zhan, Z. Wang, L. Zhang, C. Feng, and X. Shen, *J. Lightwave Technol.* **35**, 2325 (2017).
12. K. Wang and C. Xu, *Appl. Phys. Lett.* **99**, 071112 (2011).
13. N. G. Horton, K. Wang, D. Kobat, C. G. Clark, F. W. Wise, C. B. Schaffer, and C. Xu, *Nat. Photonics* **7**, 205 (2013).
14. X. Fang, Z. Q. Wang, and L. Zhan, *Opt. Eng.* **56**, 046107 (2017).
15. K. Tamura, H. A. Haus, and E. P. Ippen, *Electron. Lett.* **28**, 2226 (1992).
16. Y. Senoo, N. Nishizawa, Y. Sakakibara, K. Sumimura, E. Itoga, H. Kataura, and K. Itoh, *Opt. Express* **18**, 20673 (2010).
17. F. M. Mitschke and L. F. Mollenauer, *Opt. Lett.* **11**, 659 (1986).
18. J. P. Gordon, *Opt. Lett.* **11**, 662 (1986).
19. N. Nishizawa, R. Okamura, and T. Goto, *J. Appl. Phys.* **38**, 4768 (1999).
20. K. Tamura, E. P. Ippen, H. A. Haus, and L. E. Nelson, *Opt. Lett.* **18**, 1080 (1993).
21. G. P. Agrawal, *Nonlinear Fiber Optics* (Oxford, 2007).
22. I. A. Yarutkina, O. V. Shtyrina, M. P. Fedoruk, and S. K. Turitsyn, *Opt. Express* **21**, 12942 (2013).
23. F. O. Ilday, J. R. Buckley, W. G. Clark, and F. W. Wise, *Phys. Rev. Lett.* **92**, 213902 (2004).
24. A. Chong, J. Buckley, W. Renninger, and F. Wise, *Opt. Express* **14**, 10095 (2006).